Factors Affecting the Collection and Fitting of Nuclear Magnetic Cross-Relaxation Spectroscopy Data with Application to Waxy Corn Starch

Kenneth S. Lewen,[†] Iris H. McCormick,[‡] Paul Molitor,[§] Shelly J. Schmidt,*[,†] and Thomas M. Eads[#]

Department of Food Science and Human Nutrition, University of Illinois, 905 South Goodwin Avenue, Urbana, Illinois 61801; Warren Analytical Laboratory, 650 "O" Street, Greeley, Colorado 80632; VOICE NMR Laboratory, University of Illinois, 600 South Mathews, Urbana, Illinois 61801; and Molecular Origins, Inc., 1518 Yancey Street, Tallahassee, Florida 32303

An examination of the methods for nuclear magnetic cross-relaxation spectroscopy (CRS) data collection and analysis was conducted using water and an aqueous waxy corn starch suspension to better perform and interpret the results obtained using CRS. The CRS data collection properties evaluated were the time to achieve steady state saturation, the direct saturation of liquid protons, generation of transverse magnetization, and dependence of the offset frequency and radio frequency (RF) field strength of longitudinal relaxation in the presence of RF saturation. Effects were evaluated for variations of input values of RF saturation field strength, apparent cross-relaxation rate, and solid longitudinal relaxation rate on the results for solid content and solid internal mobility from fitting NMR data to modified theoretical expressions. Discrepancies between fitted and stoichiometric values for the solid to liquid proton ratio were investigated. The fitting procedure used a Gaussian line shape for RF saturation of the solid-like spin system and a Lorentzian line shape for RF saturation of the liquid-spin system. Conditions under which acceptable results can be obtained with limited data sets are discussed.

Keywords: *Waxy corn starch; nuclear magnetic resonance spectroscopy; NMR; cross-relaxation*

INTRODUCTION

Food materials that are semisolids, suspensions, slurries, and emulsions owe most of their functional properties to the dynamic network of bonds and molecular assemblies that make up their architecturally and rheologically important elements. To understand how functionality arises from the solid-like components, techniques are needed to selectively measure their molecular structure and dynamics in situ. Nuclear magnetic resonance (NMR) spectroscopy is the only tool that can measure the rates and amplitudes of molecular motions within the structural domains themselves (Wu et al., 1992).

Cross-relaxation spectroscopy (CRS) is a unique NMR technique that is more or less selective for solid-like components and probes molecular mobility within them using liquids rather than solids NMR instrumentation and techniques (Wolff and Balaban, 1989; Grad and Bryant, 1990). CRS also yields rate constants that may be interpreted in terms of the association of mobile molecules with solid-like phases. Because of its selectivity and sensitivity, CRS should be particularly useful in the analysis of pourable and spoonable salad dressings, puddings, gravies, sauces, soups, low-fat solid and pourable margarines, relishes and salsas, many dairy products, and other low-level solid food systems because the solids in these systems are not measurable with standard solids NMR techniques. However, applications of CRS are not limited to materials having low levels of solids; insights about solids in more concentrated systems have also been gained (Wu et al., 1992; Wu and Eads, 1993; Eads and Axelson, 1995).

CRS is based on the magnetic coupling between two distinct spin systems in which magnetization is transferred from one spin system to the other. These nuclear spin systems may couple by several possible mechanisms (Eads and Axelson, 1995): (1) magnetic dipolar coupling, in which transfer of magnetization occurs through space between nuclei (e.g., a water and a solid proton) within ~0.5 nm of each other (or between nuclei and unpaired electrons); (2) chemical exchange (or atom transfer), in which distinctly different atoms (e.g., H^+) or chemical functional groups (e.g., $-NH_3^+$) physically exchange positions (e.g., physical exchange between a free water and a labile solid proton); and (3) molecular exchange, in which whole solvent or solute molecules exchange positions within solid component cavities or binding sites and the "bulk" liquid. We are not concerned here with cross-relaxation through J-coupling or as a manifestation of the intramolecular nuclear Overhauser effect in solutes, as these are used primarily in the determination of molecular structure in solution and do not provide a basis for analysis of solids.

* Author to whom correspondence should be addressed [telephone (217) 333-6369; fax (217) 244-7877; e-mail sjs@uiuc.edu].
[†] Department of Food Science and Human Nutrition.
[‡] Warren Analytical Laboratory.
[§] VOICE NMR Laboratory.
[#] Molecular Origins, Inc.

10.1021/jf000353h CCC: $19.00
Published on Web 08/25/2000

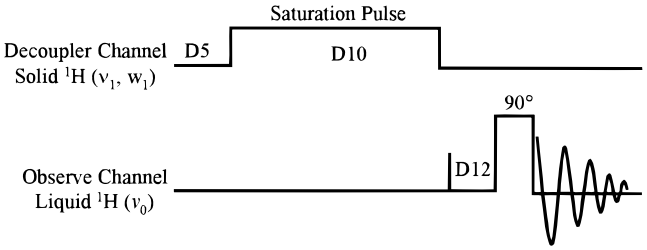

Figure 1. CRS pulse sequence. D5 = 20 s, D12 = 200 μs, D10 = 5 or 6 s depending on B_1 (experiment set 1). Five B_1 values were used, 200, 274, 417, 536, and 695 Hz, and the Δ values typically ranged from 50 to −50 kHz in 5 kHz increments, unless otherwise stated. ν_1 is the Δ at which the saturation pulse is applied. ν_0 is the Larmor frequency of the liquid spins.

The relevant consequences of coupling between nuclear spin systems are that (1) relaxation in one spin system bears some of the character of relaxation in the other and (2) it provides a mechanism for transfer of spin energy (longitudinal magnetization) or spin coherence (transverse magnetization) between the spin systems. Both of these consequences are analytically useful.

Our concern is coupling in food materials between nuclei of molecules in liquid-like domains (water and its solutes, oil and its solutes) and nuclei of molecules in solid-like domains (biomacromolecules, crystallites, liquid crystals, films, and so on). Virtually every mechanism for coupling is present in food semisolids and viscous liquids: (1) Solid and liquid spins are in intimate, atomic level contact at the solid−liquid interface, giving rise to dipolar coupling. (2) Both phases have labile hydrogens (at least in the aqueous case) giving rise to proton exchange. (3) Solvent and solute molecules may find binding sites within solid-like domains, thus coupling them by molecular exchange.

The cross-relaxation spectroscopy method is straightforward and can be executed on a wide range of NMR instruments. The CRS pulse sequence is shown in Figure 1. The CRS method involves three steps: preparation (establishing solid and liquid magnetization by immersion of the sample in a strong magnetic field); selective saturation [by radio frequency (RF) irradiation applied at a frequency, ν_1, offset from the liquid resonance, ν_0], and detection (by a 90° pulse that places liquid magnetization in the transverse plane).

The phenomenon of magnetic relaxation coupling in dynamically heterogeneous systems leaves a characteristic signature on both magnetization recovery curves (longitudinal or spin−lattice relaxation), the spectral line shape, and spin−echo decay curves, each now reflecting all processes that produce magnetic coupling (Kalk and Berendsen, 1976; Edzes and Samulski, 1978; Fung and McGaughy, 1980; Shirley and Bryant, 1982). Relaxation coupling also alters the static field dependence of the longitudinal relaxation rate [see Bryant et al. (1991), for example]. Development of CRS theory helped researchers to separate the cross-relaxation contribution to the water proton longitudinal relaxation from contributions due to water rotational and translational diffusion (Edzes and Samulski, 1978; Shirley and Bryant, 1982).

Cross-relaxation spectroscopy has been used to study a wide variety of samples, including model systems, such as agar gels (Henkelman et al., 1993) and cross-linked bovine serum albumin (Grad and Bryant, 1990; Wu, 1991); biological systems, including hydrated and natural collagen (Edzes and Samulski, 1977, 1978), heat-denatured egg albumin (Yeung and Swanson, 1992), muscle (Edzes and Samulski, 1978), and rabbit kidney (Wolff and Balaban, 1989); and food systems, including hydrated corn starch (Swanson, 1991), gelatinized waxy maize starch (Wu et al., 1992; Wu and Eads, 1993), and banana (Ni and Eads, 1992).

Depending on the spectrometer system and potential for automation, collecting enough data can be more or less time-consuming. The time for acquiring multiple cross-relaxation (CR) spectra is greatly reduced by using broadband excitation and detection (Swanson, 1991). Without gradient capability, the analyst needs to know the consequences of fitting a restricted data set to the CR theory and under what conditions a fit of the CR data to simple line shape functions (Wu et al., 1992; Wu and Eads, 1993) represents a good alternative. These analytical issues are addressed in this paper.

The objective of this research was to critically examine factors that affect the collection and fitting of limited cross-relaxation data sets obtained on samples of starch granules suspended in water. The factors to be analyzed include the duration of the RF saturation pulse, direct saturation of liquid protons caused by the off-resonance RF irradiation, residual transverse magnetization, the offset frequency dependence of apparent longitudinal relaxation, the discrepancy between stoichiometric and fit values for the solid to liquid proton ratio, and the effect of various initial choices for fixed parameter values on the results fitting CR spectra to the simplified theoretical expression of Eads and Axelson (1995). [This reference (Eads and Axelson, 1995) contains a typographical error: the numerator in the first term of their eq 2 should be $R_{BA}R'$ rather than $2R'$.]

Starch was chosen as the model food sample because it is a major ingredient consumed by humans and an excellent raw material for modifying the texture and the consistency of foods (BeMiller and Whistler, 1996). Also, starch is used in diverse applications, including pharmaceuticals, textiles, and adhesives, as well as new emerging applications, including low-calorie fat substitutes, "biodegradable" packaging materials, thin films, and thermoplastic materials (Biliaderis, 1998).

EXPERIMENTAL PROCEDURES

Sample Preparation. Two model systems were used: deionized ultrapure water (Photronix reagent grade water system distributed by Vanguard International) and ungelatinized mixtures of 10% waxy No. 1 7350 cornstarch (lot SB80848CB, A. E. Staley Manufacturing Co., Decatur, IL) and 0.25% xanthan gum (lot P.3119, TIC Gums Inc., Belcamp, MD) dispersed in deionized ultrapure water (concentrations are reported as percent dry solids). The starch mixture was prepared by first creating a homogeneous dispersion of xanthan and water in a stainless steel beaker. Cornstarch was mixed into the xanthan/water dispersion at a mixing rate of 500 rpm for 4 min, to ensure that a homogeneous dispersion is achieved, using a hoop stirrer attached to a Servodyne mixer (model E650, Electro-Craft Servo Products, Eden Prairie, MN) that was controlled by a constant-speed Servodyne mixer control unit (Cole-Parmer Instrument Co., Chicago, IL). The starch system was hydrated for a minimum of 2 h before NMR measurements were made. The function of the xanthan was to keep the starch granules homogeneously dispersed. It was assumed that the xanthan did not contribute a significant cross-relaxation signal. Therefore, the important liquid spin system is assumed to be composed of water protons plus exchangeable starch protons, and the important solid spin system is composed of nonexchangeable starch protons.

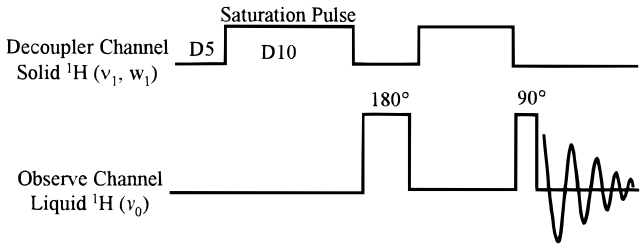

Figure 2. IR and IRSAT pulse sequences used to determine R_{BA} and R_A. D5 = 20 s, D12 = 200 μs, D10 = 5 s, B_1 = 285 Hz, and six Δ values ranging from 50 kHz to 5 kHz were used. ν_1 is the Δ at which the saturation pulse is applied. ν_0 is the Larmor frequency of the liquid spins.

The starch mixture was transferred into Ultra Precision 5 mm medium-walled NMR tubes (Wilmad Glass Co., Inc., Buena, NJ) with Pasteur pipets. The starch system was shaken before being transferred into NMR tubes to ensure homogeneous distribution of the starch granules. Medium-walled NMR tubes were used to decrease the intensity of the water signal so that the receiver would not be overloaded.

NMR Experiments. Experiments were run on a GN300WB NMR spectrometer equipped with a 7.05 T superconducting magnet, a 10 mm broadband probe, and version 12.0 of GEM software (General Electric Co. NMR Instruments, Fremont, CA). The samples were not spun because the centrifugal force generated by spinning caused the dispersed starch granules to become unevenly dispersed. The spectrometer was operated at 20 ± 1°C. To enable the spectrometer to apply the required power for the CR experiment without damaging the probe, a minor modification was made. The original 560 Ω resistor in the 300 MHz probe interface box was replaced with five 2.7 kΩ, 2 W resistors in parallel.

The CRS pulse sequence is shown in Figure 1 and consists of two pulses, a long low-power saturation pulse and a short high-power 90° detection pulse. The saturation pulse was applied via the decoupler channel at a frequency ν_1, and the 90° detection pulse, typically 31.5 ± 1 μs for water and 33.25 ± 1 μs for the starch mixture, was applied via the observe channel at the water resonance frequency, ν_0. The delay between successive experiments, D5, was 20 s, which is at least six times the longitudinal relaxation rate, T_1, for water protons, the longest T_1 in the samples. The delay between the saturation pulse and the 90° detection pulse, D12, was 200 μs. The saturation pulse duration, D10, saturation power level, B_1 (hertz), and offset frequency, $\Delta = \nu_1 - \nu_0$, of the saturation pulse were varied for different experiments. D10 was optimized for each choice of B_1. Saturation field strengths are expressed as the proton precession frequency, ω_1 (radians/second) = $2\pi B_1$, determined for each sample from the pulse time t_p to produce a tip angle, θ (radians), when B_1 is applied at the resonance frequency of water, ν_0. Δ values typically ranged from 50 to −50 kHz in 5 kHz increments, unless otherwise stated. A CR spectrum is a plot of normalized intensity of the liquid signal, M_A^{SS}/M_A^0, versus offset frequency, Δ, where M_A^{SS} and M_A^0 are the Z-magnetizations of the liquid component in the presence and absence of steady state saturation of the solid, respectively. Each experiment was at least done in duplicate.

The inversion recovery (IR) experiment is the same as the inversion recovery with saturation (IRSAT) experiment without the application of the saturation pulse on the decoupler channel. The IR and IRSAT pulse sequences are shown in Figure 2. The IR and IRSAT experiments were used to measure the apparent longitudinal relaxation and to obtain the Grad and Bryant (1990) cross-relaxation rate, R_{BA}, along with the liquid longitudinal relaxation rate, R_A.

Data Treatment. The CR spectrum was fit to the Eads and Axelson (1995) model using a least-squares approach. The typographical error in the Eads and Axelson expression is corrected in equation 1

$$1 - \frac{M_A^{SS}}{M_A^0} = \frac{R_{BA}R_{RFB}}{\frac{R_A R_{BA}}{f} + (R_{BA} + R_A)(R_B + R_{RFB})} + \frac{LA}{LW^2 + \Delta^2} \quad (1)$$

where f denotes the ratio of the number of solid protons effective in cross-relaxation to the number of liquid protons effective in cross-relaxation; R_{BA} is the cross-relaxation rate; R_A and R_B are the longitudinal relaxations in the absence of magnetization transfer rates of the liquid and solid proton populations, respectively; Δ is the offset of the saturation RF field from the center of the liquid resonance ($\nu_1 - \nu_0$); and R_{RFB}, the Gaussian line shape function, is defined in

$$R_{RFB} = T_{2B}\omega_1^2\left(\frac{\pi}{2}\right)^{1/2} \exp\left[-\frac{(2\pi\Delta T_{2B})^2}{2}\right] \quad (2)$$

where T_{2B} is the transverse relaxation time for the solid proton population and ω_1 is the proton precession frequency in the RF field of the saturation pulse. The Lorentzian term, $LA/LW^2 + \Delta^2$, accounts for the narrow component at the center of the CR spectrum. LA is the amplitude (Hz^2) and LW is the width (Hz) of the narrow Lorentzian, determined during the fitting process. This is equivalent to the Lorentzian expression used by Eads and Axelson (1995), $C/[1 + (2\Delta/\Delta\nu_{1/2})^2]$, where C is the intensity parameter and $\Delta\nu_{1/2}$ is the width at half-height of the narrow Lorentzian; therefore, $C = LA/LW^2$ and $2LW = \Delta\nu_{1/2}$.

The Eads and Axelson model is similar to the Grad and Bryant (1990) model with two adjustments: (1) the Lorentzian form of R_{RFB} was replaced with a Gaussian function that better describes the solid-like spin system (Swanson, 1992) and (2) a Lorentzian function was added to fit the narrow component of the CR spectrum at small offset frequencies (Wu, 1991; Caines et al., 1991).

Equations 1 and 2 were programmed into Excel Visual Basic (Microsoft Co., Seattle, WA), and the data were fit through a least-squares approach. Of the 11 parameters in the CR model, the values for ω_1 (= $2\pi B_1$) and Δ are known and M_A^{SS} and M_A^0 are determined from the CRS experiment. Because the seven remaining parameters are more than can be obtained uniquely by fitting, it is necessary to obtain two or more of the parameters independently. R_A and R_{BA} were determined using the IR and IRSAT experiments as outlined by Grad et al. (1990). The IRSAT data were fit to

$$M'(t) = \frac{M_\infty - M(t)}{2M_\infty} = \left[M'(t=0) - \frac{R_{BA}}{2(R_{BA} + R_A)}\exp[-(R_{BA} + R_A)t] + \frac{R_{BA}}{2(R_{BA} + R_A)}\right] \quad (3)$$

where $M'(t)$ is the normalized magnetization, $M(t)$ is the magnetization at time t, and M_∞ is measured using the IR experiment at a value of t that is much greater than the T_1 of water. This expression is equivalent to the one used by Grad et al. (1990) and is in the form given by Eads and Axelson (1995).

R_B was assigned on the basis of literature values for similar systems and does not have a significant influence on the final fit. This leaves four unknowns, f, T_{2B}, LA, and LW. Approximate values for these unknowns are entered as starting points for the fitting procedure based on our knowledge of the sample system. If poor choices are made for these values, then poor fits may result.

The most important parameters for the study of foods are f, a measure of solid in contact with liquid; T_{2B}, a measure of the internal mobility of solid-like domains; R_{BA}, a measure of

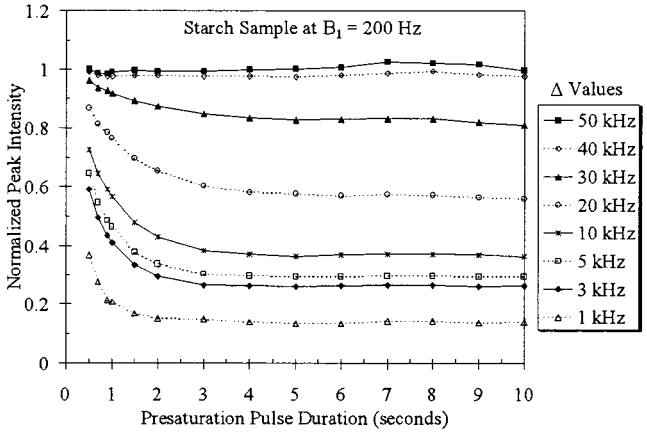

Figure 3. Steady state saturation for the ungelatinized starch sample determined by plotting the normalized peak intensity as a function of 14 saturation pulse lengths 0.5−10 s at 8 Δ values varying from 50 to 1 kHz with $B_1 = 200$ Hz.

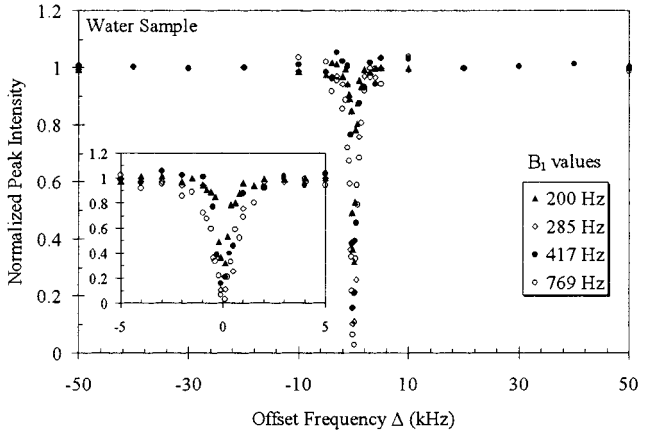

Figure 4. Detection of direct saturation of the liquid protons by the saturation pulse at four B_1 values, 200, 285, 417, and 769 Hz, and Δ values between ±50 kHz. (Inset) Same plot with Δ values between ±5 kHz.

concentration-dependent accessibility of the solid to the liquid; R_B and R_A are difficult to interpret unambiguously.

RESULTS AND DISCUSSION

Approach to Steady-State Partial Saturation. The CR model (eq 1) is valid only when steady state saturation is achieved. The duration necessary to achieve steady state at five B_1 amplitudes from 200 to 695 Hz and eight offset frequencies Δ from 50 to 1 kHz were determined. The approach to steady state is shown in Figure 3 for B_1 of 200 Hz. Steady state saturation occurs when the normalized peak intensity reaches a constant value as Δ increases as shown in Figure 3. A 5 s pulse length is required to reach steady state saturation for all B_1 values, except a length of 6 s is required for the lowest value of 200 Hz.

The shapes of the curves in Figure 3 are due to several factors. During the saturation pulse, RF magnetization partially saturates the solid protons. At the same time, cross-relaxation, longitudinal, and transverse relaxations are occurring, which causes the magnetization to return to equilibrium. When $R_{BA} \geq R_A$, some magnetization is transferred from the solid to the liquid protons, resulting in an indirect saturation of the liquid and a decrease in the water proton peak as measured by the 90° detection pulse.

The rates at which steady state are reached depend on the B_1 and Δ used. The stronger B_1, the more quickly will steady state be reached. The CR spectrum is a reflection of the number of saturated solid protons. Therefore, at very large Δ values (i.e., 40−50 kHz), the solid protons are slightly saturated, thereby the resulting liquid signal is barely distinguishable from the noise. As Δ decreases, the amount of solid protons that are saturated increases, resulting in a greater transfer of magnetization to the liquid protons as observed by an increase in the CR spectrum. However at Δ < 10 kHz, the water protons are not only indirectly saturated, they are directly saturated, thereby rapidly increasing the CR spectrum and resulting in the fastest apparent steady state saturation rate.

Direct Saturation of the Liquid Protons. Experimental CRS measurements for the water sample are shown in Figure 4 at B_1 levels of 200, 285, 417, and 769 Hz. A magnitude calculation was done to obtain the peak heights. The CR spectra result from the direct saturation of the liquid protons by the saturation pulse.

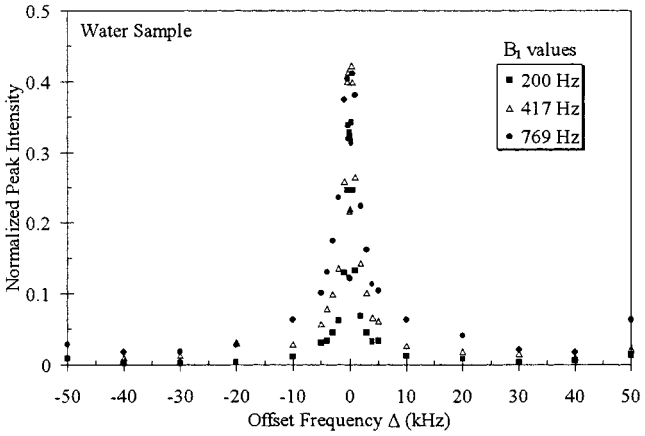

Figure 5. Determination of any induced tranverse magnetization by the saturation pulse using CRS without the 90° detection pulse on the water sample at three B_1 values, 200, 417, and 769 Hz, and Δ values between ±50 kHz.

This is the region that is fit by the narrow Lorentzian component, $LA/(LW^2 + \Delta^2)$.

Even though there is slight variability in the data, the precision provided by this experiment is sufficient to determine that direct saturation occurs between Δ = ±10 kHz at the specified power levels. These results show the importance of either including a narrow Lorentzian component in the CR model or excluding this region when one is fitting a CR model that does not account for the direct saturation of the liquid spins. A suggestion to decrease the variability is to vary the order of Δ values during data acquisition (Stephans and Foster, 1998).

Transverse Magnetization Effects Caused by the Saturation Pulse. Because phase cycling will double the acquisition time, this set of experiments was done to determine if the residual transverse magnetization was significant. To determine this, the CRS pulse sequence at B_1 levels of 200, 417, and 769 Hz was used with the omission of the 90° read pulse. The FID was zero filled before transformation, and the peak intensities were obtained after application of a magnitude calculation. The normalized intensities were plotted as a function of Δ at the three B_1 values and are shown in Figure 5 for water and in Figure 6 for starch.

A significant amount (≥0.25 of the value for the noise) of transverse magnetization is seen for the water

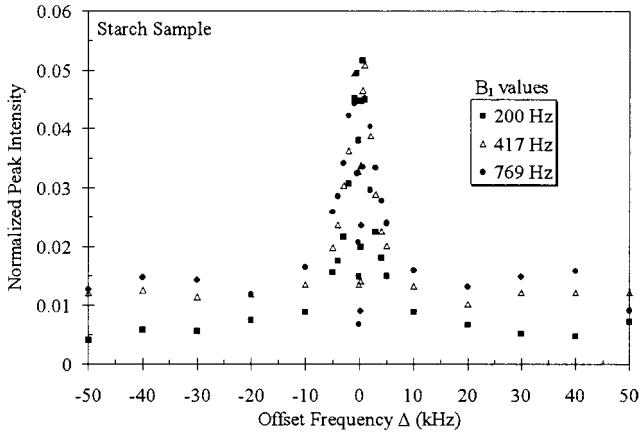

Figure 6. Determination of any induced tranverse magnetization by the saturation pulse using CRS experiment without the 90° pulse on the starch sample at three B_1 values, 200, 417, and 769 Hz, and Δ values between ±50 kHz.

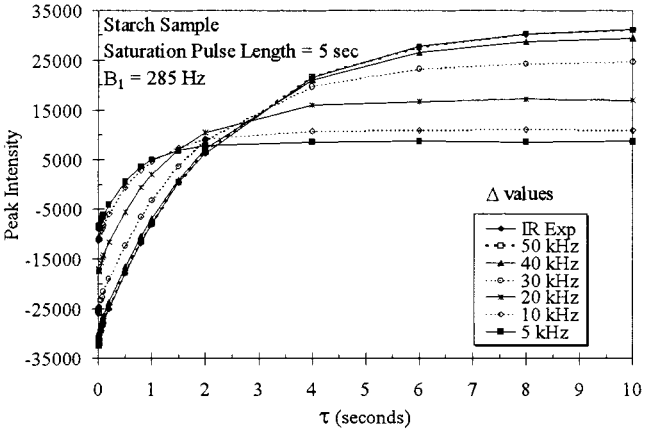

Figure 7. Peak intensities of the IR and IRSAT experiments for the starch sample plotted as a function of 19 τ values, ranging from 0.001 to 10 s. The IRSAT experiment was done at 6 Δ values ranging from 50 to 5 kHz using a 5 s and a saturation pulse of 285 Hz.

sample. However, due to the effects of cross-relaxation and lower concentration of water in the starch sample, an insignificant amount of transverse magnetization was observed, approximately $^1/_{10}$ the strength of the signal seen for the water sample. Therefore, for the purposes of the starch sample, transverse magnetization does not play a significant role. If transverse magnetization was significant, there would be a number of techniques that can be used to eliminate its effects, such as phase cycling (Henkelman et al., 1993) and the use of homospoiling gradient pulses (Grad and Bryant, 1990).

Validity of Using the IRSAT Experiment for Determining R_{BA} and R_A. The values for R_{BA} and R_A are determined using the IR and IRSAT experiments and fit to eq 3. Because eq 3 is not a function of Δ, only one Δ can be fit at a time. The validity of choosing just one Δ was examined using an ungelatinized starch sample, six Δ values ranging from 50 to 5 kHz, and a 5 s, 285 Hz saturation pulse. Figure 7 is a plot of peak intensity as a function of time (t) for both the IR and IRSAT experiments.

The change in R_{BA} as a function of Δ was drastic, as is shown in Figure 8. R_{BA} varied from values as high as 1.13 s^{-1} for 5 kHz to as low as 0.00073 s^{-1} for 50 kHz. This occurred because R_{BA} is not a fundamental rate

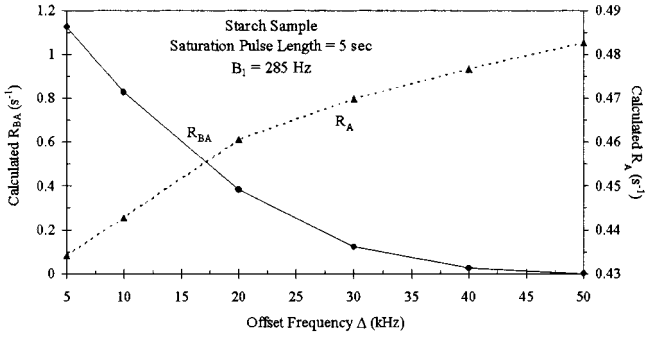

Figure 8. Relationship between R_{BA} and R_A plotted as a function of Δ. The IR and IRSAT experiments were done on the starch sample at 19 τ values, ranging from 0.001 to 10 s. The IRSAT experiment was done at 6 Δ values ranging from 50 to 5 kHz using a 5 s and a saturation pulse of 285 Hz.

constant but a "pseudo rate" constant that cannot be described by a single value at which it is valid for all values of Δ. R_{BA} is a measure of the amount of magnetization transferred in a given amount of time from the solid protons to the liquid protons. Therefore, the amount of magnetization transferred increases as the number of saturated solid protons increases as observed by a decrease in Δ. To a lesser degree, the opposite effect happens to R_A. As Δ is decreased, more solid protons are available to participate in cross-relaxation. In this case, cross-relaxation is a faster pathway than longitudinal relaxation; thus, the liquid protons will relax via the cross-relaxation pathway. Therefore, as Δ is decreased, the efficiency of R_A decreases because more liquid protons are participating in CR.

Therefore, this experiment set elucidates a weakness in the CR model because R_{BA} and R_A vary significantly with Δ. The dependence of the calculated R_{BA} value on the offset frequency of the IRSAT experiment illustrates that the rate of magnetization transfer during the CR experiment cannot be described by a single value which would be valid over the whole offset frequency range of the CR spectrum.

Henkelman et al. (1993) argued that reliable fits and stable parameters could not be obtained at just one B_1 but that a global fit of several CR spectra at different B_1 values is needed. We concur with this finding but suggest that the method used in this paper is a practical alternative when a method for rapid CR data is not available, for example, broadband CRS (Swanson, 1991). After R_A and R_{BA} are obtained from the IR and IRSAT experiments (values given in Table 1), the fit of the CR spectra to eq 1 becomes straightforward. The importance of this CR method is not to obtain "true" values for the parameters but to attain values for the parameters that can be compared to those obtained using a similar sample. For example, this method could be used to study changes in samples over time, for example, the retrogradation of starch (Wu and Eads, 1993).

Effect of B_1, IRSAT Δ, R_B and the Narrow Lorentzian on the Fitting of the CR Model. To use this cross-relaxation technique effectively, the limits under which the CR spectra-fitting function is valid need to be determined. The limits of the CR fitting function were explored by determining how three variables, B_1, IRSAT Δ, and R_B, and the inclusion of the narrow Lorentzian affect the fitting results of f and T_{2B}.

The experiments were done on the starch sample. Two replications of nine unique CR experiments were run

Table 1. R_{BA} and R_A Values Determined by Fitting the IRSAT Data to Equation 3[a]

	Δ = 10 kHz			Δ = 25 kHz			Δ = 40 kHz		
B_1	695 Hz	417 Hz	200 Hz	695 Hz	417 Hz	200 Hz	695 Hz	417 Hz	200 Hz
R_{BA} (s^{-1})	1.45 ± 0.016	1.17 ± 0.033	0.58 ± 0.017	0.52 ± 0.035	**0.36 ± 0.012**	**0.17 ± 0.017**	**0.10 ± 0.009**	**0.07 ± 0.010**	**0.02 ± 0.027**
R_A (s^{-1})	0.40 ± 0.024	0.43 ± 0.009	0.43 ± 0.016	0.43 ± 0.014	**0.45 ± 0.017**	**0.44 ± 0.010**	**0.46 ± 0.003**	**0.45 ± 0.011**	**0.46 ± 0.024**

[a] The experiments were done at three Δ values and three B_1 values. The regions shown in boldface type are unrealistic fits ($f_{obs} > f_{stoichiometric} = 0.044$).

Table 2. Results from Fitting the CR Data, *including* the Narrow Lorentzian Region (Δ = ±10 kHz), to Equation 1 *with* the Lorentzian Line Shape Function[a]

		Δ = 10 kHz			Δ = 25 kHz			Δ = 40 kHz		
R_B (s^{-1})	B_1	695 Hz	417 Hz	200 Hz	695 Hz	417 Hz	200 Hz	695 Hz	417 Hz	200 Hz
0.1	f	0.0077 ± 0.0014	0.025 ±0.002	**0.061 ± 0.017**	0.018 ± 0.004	**0.49 ± 0.46**	**1.00 ± 0.00**	**1.00 ± 0.00**	**1.00 ± 0.00**	**1.00 ± 0.00**
	T_{2B} (×10^5 s)	1.11 ± 0.005	1.22 ± 0.02	**1.39 ± 0.04**	1.27 ± 0.05	**1.63 ± 0.19**	**1.95 ± 0.01**	**1.89 ± 0.05**	**1.92 ± 0.02**	**1.25 ± 1.44**
	fit error %	0.79 ± 0.13	1.03 ± 0.12	**3.25 ± 0.16**	1.59 ± 0.35	**2.90 ± 0.63**	**5.49 ± 0.51**	**7.21 ± 0.85**	**7.88 ± 1.10**	**11.1 ± 3.1**
1.0	f	0.0079 ± 0.0015	0.027 ± 0.002	**0.078 ±0.027**	0.027 ± 0.013	**1.00 ± 0.00**	**1.00 ± 0.00**	**1.00 ± 0.00**	**1.00 ± 0.00**	**1.00 ± 0.00**
	T_{2B} (×10^5 s)	1.11 ± 0.005	1.22 ± 0.02	**1.39 ± 0.04**	1.30 ± 0.08	**1.61 ± 0.02**	**1.60 ± 0.004**	**1.66 ± 0.04**	**1.64 ± 0.01**	**1.61 ± 0.01**
	fit error %	0.79 ± 0.13	1.03 ± 0.12	**3.28 ± 0.14**	1.80 ± 0.60	**2.63 ± 0.11**	**5.70 ± 0.69**	**7.52 ± 0.88**	**8.3 ± 1.14**	**11.2 ± 2.7**
10	f	0.010 ± 0.002	**0.54 ± 0.53**	**1.00 ± 0.00**	**1.00 ± 0.00**	**1.00 ± 0.00**	**1.00 ± 0.00**	**1.00 ± 0.00**	**1.00 ± 0.00**	**1.00 ± 0.00**
	T_{2B} (×10^5 s)	1.11 ± 0.005	**1.24 ± 0.04**	**1.15 ± 0.02**	**1.32 ± 0.00**	**1.23 ± 0.006**	**1.18 ± 0.08**	**1.34 ± 0.03**	**1.28 ± 0.01**	**6.70 ± 7.65**
	fit error %	0.79 ± 0.13	**1.08 ± 0.06**	**5.35 ± 0.76**	**1.73 ± 0.19**	**3.30 ± 0.76**	**8.44 ± 0.84**	**9.04 ± 0.88**	**10.2 ± 1.1**	**11.1 ± 3.7**

[a] The regions shown in boldface type are unrealistic fits ($f_{obs} > f_{stoichiometric} = 0.044$).

Table 3. Results from Fitting the CR Data, *excluding* the Narrow Lorentzian Region (Δ = ± 10 kHz), to Equation 1 *without* the Lorentzian Line Shape Function[a]

		Δ = 10 kHz			Δ = 25 kHz			Δ = 40 kHz		
R_B (s^{-1})	B_1	695 Hz	417 Hz	200 Hz	695 Hz	417 Hz	200 Hz	695 Hz	417 Hz	200 Hz
0.1	f	0.008 ± 0.0016	0.027 ± 0.003	**0.056 ± 0.019**	0.043 ± 0.021	**0.57 ± 0.33**	**1.00 ± 0.00**	**1.00 ± 0.00**	**1.00 ± 0.00**	**1.00 ± 0.00**
	T_{2B} (×10^5 s)	1.12 ± 0.008	1.23 ± 0.03	**1.35 ± 0.04**	1.37 ± 0.08	**1.62 ± 0.06**	**1.76 ± 0.03**	**1.51 ± 0.02**	**1.43 ±0.01**	**1.16 ± 0.25**
	fit error %	0.57 ± 0.21	0.40 ± 0.18	**0.16 ± 0.12**	3.0 ± 1.5	**8.8 ± 3.9**	**5.4 ± 1.8**	**88 ± 2**	**85 ± 12**	**56 ± 25**
1.0	f	0.008 ± 0.0017	0.029 ± 0.004	**0.080 ± 0.028**	**0.054 ± 0.030**	**0.86 ± 0.29**	**1.00 ± 0.00**	**1.00 ± 0.00**	**1.00 ± 0.00**	**1.00 ± 0.00**
	T_{2B} (×10^5 s)	1.12 ± 0.008	1.23 ± 0.03	**1.37 ± 0.04**	**1.37 ± 0.08**	**1.49 ± 0.03**	**1.41 ± 0.03**	**1.29 ± 0.02**	**1.17 ± 0.02**	**0.88 ± 0.18**
	fit error %	0.57 ± 0.21	0.40 ± 0.18	**0.20 ± 0.11**	**3.0 ± 1.5**	**8.6 ± 4.4**	**7.1 ± 2.0**	**89 ± 20**	**87 ± 12**	**58 ± 24**
10	f	0.011 ± 0.003	**0.21 ± 0.12**	**1.00 ± 0.00**	**1.00 ± 0.00**	**1.00 ± 0.00**	**1.00 ± 0.00**	**1.00 ± 0.00**	**1.00 ± 0.00**	**1.00 ± 0.00**
	T_{2B} (×10^5 s)	1.12 ± 0.008	**1.23 ± 0.03**	**1.07 ± 0.04**	**1.15 ± 0.27**	**1.07 ± 0.03**	**0.91 ± 0.006**	**0.96 ± 0.009**	**0.81 ± 0.01**	**0.89 ± 0.24**
	fit error %	0.57 ± 0.21	**0.40 ± 0.18**	**4.1 ± 2.2**	**22 ± 38**	**19 ± 7**	**22 ± 3**	**98 ± 1**	**99 ± 12**	**45 ± 31**

[a] The regions shown in boldface type are unrealistic fits ($f_{obs} > f_{stoichiometric} = 0.044$).

using three B_1 values (200, 417, and 695 Hz) and three IRSAT Δ values (10, 25, and 40 kHz). Three R_B values (0.1, 1.0, and 10 s^{-1}) were selected, on the basis of reasonable literature values, to complete the design. A central composite parameter design was used to ensure all possible combinations were performed (Montgomery, 1991). The resulting 54 (3 × 3 × 3 × 3 × 2) CR spectra were fit to the CR model (eq 1), and the resulting values for f and T_{2B} were averaged over the replicates and are shown in Table 2. Finally, data within ±10 kHz were excluded and the narrow Lorentzian was given a value of 0 and therefore removed from the CR fitting equation (eq 1). The data were then fit to the modified CR model given in eq 1, and the resulting values for f and T_{2B} were averaged over the replicates and are shown in Table 3.

Basis for Choosing R_B. R_B values of 0.1, 1.0, and 10 s^{-1} were chosen instead of determining them experimentally for several reasons. First, solid state NMR needs to be used to determine R_B directly, which requires specialized equipment. Because the purpose of this experiment set was to determine the effect that different R_B values have on the fitting, an accurate value was not needed. Finally, because CR spectroscopy is supposed to be a technique in which solids information can be determined without the need for solids NMR, the validity of using an approximate R_B value is tested here.

The R_B values used were based on literature values, as well as the inherent constraints of the spectral data. Adamic and Blinc (1968) found R_1 values for potato amylopectin, wheat amylopectin, and native maize starch of ∼4.0, 5.6, and 8.3 s^{-1}, respectively, at 20 °C. Tanner et al. (1991) reported R_1 values of ∼1.1 and 2.7 s^{-1} for native waxy maize starch containing, respectively, 10 and 18% moisture. Therefore, three R_B values were chosen that differed by 2 orders of magnitude, 0.1, 1.0, and 10 s^{-1}.

Effect of IRSAT Δ, B_1, and R_B on Fitting of the CR Spectra. All three of the input parameters have a significant effect on the fitting of the CR spectra. To determine the accuracy of a fit, the values for f and T_{2B} are analyzed as well as the fitting error percent (Tables 2 and 3). Fits were considered "unrealistic" (areas shown in boldface type) when the values obtained for f were greater than the stoichiometric value of f (0.044), because it is not possible for a greater number of solid protons than are actually in the sample to participate in cross-relaxation.

The values of R_{BA} and R_A are directly related to the accuracy of the fit and results. Grad and Bryant (1990) stated that R_{BA} must be of the same order of magnitude or greater than R_A in order for the CR experiment to contain information about the solid component. They go on to say that when $R_{BA} \gg R_A$, the CR spectrum will give an increasingly accurate measure of the solid component. This means that better fits will be obtained when $R_{BA} \gg R_A$.

Because R_{BA} and R_A are determined from the fitting of the IR and IRSAT experiments, an explanation of the

fitting results as a function of IRSAT Δ can be explained using the Grad and Bryant limitations. When $\Delta = 25$ and 40 kHz, almost all of the fits were unrealistic except for a couple of instances at $\Delta = 25$ kHz when $B_1 = 695$ Hz and $R_B \leq 1.0\ s^{-1}$ and the narrow Lorentzian function was used. At the lower power levels, $R_{BA} < R_A$ and, in some cases, $R_{BA} \ll R_A$ (Table 1), therefore resulting in unrealistic fits. If unreasonable fits were obtained at $\Delta = 10$ kHz, it would more likely be due to one of the other parameters. Typically, a $\Delta = 10$ kHz for the IRSAT is the best choice.

Not only does changing the IRSAT Δ have an effect on the fitting, but so do changes in B_1 and R_B. As B_1 is increased, the values obtained for f and T_{2B} decrease. Also, as B_1 increases, R_{BA} increases and R_A decreases slightly, which should lead to better fits. However, if B_1 is too big, destruction of the solid lattice may occur, causing invalid results.

As R_B increases, the values obtained for f increase and the value of T_{2B} does not change much. This increase in f is negligible when going from 0.1 to 1.0 s^{-1}, but it is more pronounced when R_B is increased to 10 s^{-1}. This may mean that the limit of R_B is $\sim$10 s^{-1}.

To Use a Lorentzian or Not To Use a Lorentzian. To determine if the Lorentzian line shape function improved the fit, the CR data, including the narrow Lorentzian region ($\Delta = \pm 10$ kHz), were first fit to eq 1 with the Lorentzian line shape function. The CR data, excluding the narrow Lorentzian region ($\Delta = \pm 10$ kHz), were then fit to eq 1 without the Lorentzian line shape function. Tables 2 and 3 are the results of fit including and excluding the Lorentzian line shape function, respectively. For the most part, the fitted results were not significantly different when $\Delta = 10$ kHz, as should be expected. The fitting error percent was only marginally better when the Lorentzian line shape function was excluded. Therefore, either approach is satisfactory.

CONCLUSIONS

The purpose of this work was to determine the factors affecting the collection and fitting of cross-relaxation spectroscopy data for the purpose of comparing similar samples when advanced equipment is not available for obtaining numerous spectra in a relatively short time (e.g., gradient coil). Five experimental sets were used to do this. If desired, a narrow Lorentzian line shape function is needed to obtain an adequate fit of the region within ± 10 kHz. The effects of transverse magnetization were not large for the ungelatinized starch sample, but if they were found to be significant, phase cycling would need to be used. The effects of choosing a Δ value at which the IRSAT experiment was done greatly affected the fitted R_{BA} and R_A values. The input parameters, B_1, IRSAT Δ, and R_B, have a significant effect on the fitting procedure. The best fits were achieved for higher B_1 values (695 Hz), an IRSAT $\Delta = 10$ kHz, and a R_B value of $\approx$1. The inclusion or exclusion of the Lorentzian line shape function and the region of $\Delta = \pm 10$ kHz is negligible. Similar results were obtained with each method.

Henkelman et al. (1993) argued that reliable fits and stable parameters could not be obtained at just one B_1 but that a global fit of several CR spectra at different B_1 values is needed. We concur with this finding but suggest that the method used in this paper is a practical alternative when a method for rapid CR data is not available, for example, broadband CRS (Swanson, 1991). It is important to remember when using the CR experiment and model outlined in this paper that the R_{BA} value obtained is only a "pseudo rate" constant. Therefore, to quantitatively compare the CR model parameters obtained, the samples being analyzed must be similar, for example, measurement of a sample that changes over time (the retrogradation of a 10% starch sample or the aging of a banana), and the sample results to be compared must be collected under the same Δ and B_1 values.

ABBREVIATIONS USED

$\Delta\nu_{1/2}$	width at half-height of the narrow Lorentzian (Hz)
Δ	offset frequency $= \nu_1 - \nu_0$ (s)
ν_0	frequency of liquid resonance (Hz)
ν_1	frequency for application of saturation pulse (Hz)
ω_1	proton precession frequency (rad/s)
B_1	saturation power level (Hz)
C	intensity parameter of the narrow Lorentzian
CR	cross-relaxation
CRS	cross-relaxation spectroscopy
D10	saturation pulse duration (s)
D12	delay between the saturation pulse and the 90° detection pulse (s)
D5	delay between successive experiments (s)
f	ratio of the number of solid protons effective in cross-relaxation to the number of liquid protons effective in cross-relaxation
IR	inversion recovery
IRSAT	inversion recovery with saturation
LA	amplitude of the narrow Lorentzian (Hz^2)
LW	width of the narrow Lorentzian (Hz)
M_A^{SS}	Z-magnetization of the liquid component in the presence absence of steady-state saturation of the solid
M_A^0	Z-magnetizations of the liquid component in the absence of steady state saturation of the solid
R_A	longitudinal relaxation in the absence of magnetization transfer rates of the liquid proton population (s^{-1})
R_B	longitudinal relaxation in the absence of magnetization transfer rates of the solid proton population (s^{-1})
R_{BA}	cross-relaxation rate (s^{-1})
R_{RFB}	Gaussian line shape function (s^{-1})
t	time
T_1	longitudinal relaxation rate (s)
T_{2B}	transverse relaxation time for the solid proton population (s)

ACKNOWLEDGMENT

Our thanks and appreciation are given to Mr. Joseph Smith and Dr. Gary A. Day, Kellogg Co., who wrote and fine-tuned the spectra-fitting program used in this work.

LITERATURE CITED

Adamic, K.; Blinc, M. Proton Spin−Lattice Relaxation Time Measurements in Starch. *Polym. Lett.* **1968**, *6*, 303−305.

BeMiller, J. N.; Whistler, R. L. Carbohydrates. In *Food Chemistry*; Fennema, O. R., Ed.; Dekker: New York, 1996; pp 69−137.

Biliaderis, C. G. Structures and Phase Transitions of Starch Polymers. In *Polysaccharide Association Structures in Food*; Walter, R. H., Ed.; Dekker: New York, 1998; pp 57−168.

Bryant, R. G.; Mendelson, D. A.; Lester, C. C. The Magnetic Field Dependence of Proton Spin Relaxation in Tissues. *Magn. Reson. Med.* **1991**, *21*, 117−126.

Caines, G. H.; Schleich, T.; Rydzewski, J. M. Incorporation of Magnetization Transfer into the Formalism for Rotating-Frame Spin−Lattice Proton NMR Relaxation in the Presence of an Off-Resonance-Irradiation Field. *J. Magn. Reson.* **1991**, *95*, 558−566.

Eads, T. M.; Axelson, D. E. Nuclear Cross Relaxation Spectroscopy and Single Point Imaging Measurements of Solids and Solidity in Foods. In *Magnetic Resonance in Food Science*; Belton, P. S., Delgadillo, I., Gil, A. M., Webb, G. A., Eds.; The Royal Society of Chemistry: Cambridge, U.K., 1995; pp 230−242.

Edzes, H. T.; Samulski, E. T. Cross Relaxation and Spin Diffusion in the Proton NMR of Hydrated Collagen. *Nature* **1977**, *265*, 521−522.

Edzes, H. T.; Samulski, E. T. The Measurement of Cross Relaxation Effects in the Proton NMR Spin−Lattice Relaxation of Water in Biological Systems: Hydrated Collagen and Muscle. *J. Magn. Reson.* **1978**, *31*, 207−299.

Fung, B. M.; McGaughy, T. W. Cross Relaxation in Hydrated Collagen. *J. Magn. Reson.* **1980**, *39*, 413−420.

Grad, J.; Bryant, R. G. Nuclear Magnetic Cross Relaxation Spectroscopy. *J. Magn. Reson.* **1990**, *90*, 1−8.

Grad, J.; Mendelson, D.; Hyder, F.; Bryant, R. G. Direct Measurements of Longitudinal Relaxation and Magnetization Transfer in Heterogeneous Systems. *J. Magn. Reson.* **1990**, *86*, 416−419.

Henkelman, R. M.; Huang, X.; Xiang, Q.-S.; Stanisz, G. J.; Swanson, S. D.; Bronskill, M. J. Quantitative Interpretation of Magnetization Transfer. *J. Magn. Reson. Med.* **1993**, *29*, 759−766.

Kalk, A.; Berendsen, H. J. C. Proton Magnetic Relaxation and Spin Diffusion in Proteins. *J. Magn. Reson.* **1976**, *24*, 343−366.

Montgomery, D. C. *Design and Analysis of Experiments*, 3rd ed.; Wiley: New York, 1991.

Ni, Q. W.; Eads, T. M. Low-Speed Magic-Angle-Spinning Carbon-13 NMR of Fruit Tissue. *J. Agric. Food Chem.* **1992**, *40*, 1507−1513.

Shirley, W. M.; Bryant, R. G. Proton-Nuclear Spin Relaxation and Molecular Dynamics in the Lysozyme-Water System. *J. Am. Chem. Soc.* **1982**, *104*, 2910−2918.

Stephans, L. E.; Foster, N. Magnetization-Transfer NMR Analysis of Aqueous Poly (Vinyl Alcohol) Gels-Effect of Hydrolysis and Storage Temperature on Network Formation. *Macromolecules* **1998**, 31(5), 1644−1651.

Swanson, S. D. Broadband Excitation and Detection of Cross Relaxation NMR Spectra. *J. Magn. Reson.* **1991**, *95*, 615−618.

Swanson, S. D. Transient and Steady-State Effects of Indirect RF Saturation in Heterogeneous Systems. In *Book of Abstracts, Annual Meeting, Society for Magnetic Resonance in Medicine*; Berlin, Germany, 1992; p 255.

Tanner, S. F.; Hills, B. P.; Parker, R. Interactions of Sorbed Water with Starch Studied using Proton Nuclear Magnetic Resonance Spectroscopy. *J. Chem. Soc., Faraday Trans.* **1991**, *87*, 2613−2621.

Wolff, S. D.; Balaban, R. S. Magnetization Transfer Contrast (MTC) and Tissue Water Proton Relaxation *in Vivo*. *Magn. Reson. Med.* **1989**, *10*, 135−144.

Wu, J. Y.; Eads, T. M. Evolution of Polymer Mobility during aging of Gelatinized Waxy Maize Starch: A Magnetization Transfer ^{1}H NMR Study. *Carbohydr. Polym.* **1993**, *20*, 51−60.

Wu, J. Y.; Bryant, R. G.; Eads, T. M. Detection of Solidlike Components in Starch Using Cross Relaxation and Fourier Transform Wide-Line ^{1}H NMR Methods. *J. Agric. Food Chem.* **1992**, *40*, 449−455.

Wu, X. Line shape of Magnetization Transfer via Cross relaxation. *J. Magn. Reson.* **1991**, *94*, 186−190.

Yeung, H. N.; Swanson, S. D. Transient Decay of Longitudinal Magnetization in Heterogeneous Spin Systems under Selective Saturation. *J. Magn. Reson.* **1992**, *99*, 466−479.

Received for review March 17, 2000. Revised manuscript received July 10, 2000. Accepted July 10, 2000. NMR data were obtained in the Varian Oxford Instrument Center for Excellence in NMR Laboratory at the University of Illinois. Funding for this instrumentation was provided in part from the W. M. Keck Foundation, the National Institutes of Health (PHS 1 S10 RR10444-01), and the National Science Foundation (NSF CHE 96-10502).

JF000353H